Progress In Electromagnetics Research B, Vol. 85, 143–161, 2019

A Novel Gain-Enhanced Antenna with Metamaterial Planar Lens for Long-Range UHF RFID Applications

Edmilson C. Moreira[1, 2, *], Rodrigo O. Martins[1], Bruno M. S. Ribeiro[1], and Antônio S. B. Sombra[3, 4]

Abstract—A novel gain-enhanced microstrip antenna (MSA) with metamaterial planar lens for long-range radio frequency identification (RFID) applications for the 902–928 MHz UHF frequency band is proposed in this paper. The antenna is a combination of a new general-purpose circularly polarized MSA and a novel effective negative refractive index metamaterial (NIM) slab of 25 unit cells, arranged in a 5×5 layout, working as a planar lens for gain enhancement. The general-purpose MSA has an impedance frequency band of 828–1015 MHz, a maximum gain of 8.43 dBi at 915 MHz, an axial ratio frequency band of 896–931 MHz, and excellent performance for short and medium range RFID applications. The new infinite periodicity NIM slab has a negative refractive band of 886–1326 MHz, a negative electric permittivity band of 888–3406 MHz, and a negative magnetic permeability of band 885–1065 MHz. Together, the general-purpose MSA and the NIM planar lens results in the low-cost gain-enhanced antenna for long-range RFID applications, with an 843–993 MHz impedance frequency band and a maximum broadside gain enhancement of 48.27%, resulting in a 12.5 dBi gain at 902 MHz. Finally, the parametric studies conducted during the design process of the gain-enhanced antenna with metamaterial planar lens are presented.

1. INTRODUCTION

RFID is an Auto Identification and Data Capture (AIDC) system that carries information around using radiofrequency waves that presented a global revenue of 11.2 billion dollars in 2017 [1, 2]. This technology, especially the specified by ISO 18000-6c and operating at the ITU Region 2 frequency band, 902–928 MHz [3], has been increasingly adopted in sectors like apparel retail, assets and supply chain management, logistics and transports [4–7]. Microstrip antennas (MSA) are used in several wireless applications, being present in aircrafts, spacecrafts, missiles and satellites, for example [8]. These, according to [8–11], are thin, lightweight, cheap, easy to manufacture, to polarize circularly and linearly and to integrate with feeding networks and impedance matching structures. All these features made the MSA the most popular one for RFID readers operating in the UHF band [12]. Commonly, MSA presents gains ranging from 6–9 dBi, according to [8, 12, 13], being it sufficient for the use of RFID in medium and short range applications like apparel, retail and supply chain management, for instance [6, 7]. Nevertheless, several long-range RFID applications like the automatic identification of cars and trucks in tolls and parking spaces, as seen in [4, 5], require long-range RFID communication. In those situations, the use of high gain antennas (≥ 9 dBi) is a standard solution.

Received 15 August 2019, Accepted 23 September 2019, Scheduled 3 October 2019

* Corresponding author: Edmilson C. Moreira (edmilson.moreira@ifce.edu.br).

[1] LEMA — Laboratório de Eletromagnetismo Aplicado, Instituto Federal de Educação, Ciência e Tecnologia do Ceará, Tauá, CE, Brazil. [2] Departamento de Engenharia de Teleinformática, Universidade Federal do Ceará, Fortaleza, CE, Brazil. [3] LOCEM — Laboratório de Telecomunicações e Ciência e Engenharia de Materiais, Departamento de Física, Universidade Federal do Ceará, Fortaleza, CE, Brazil. [4] Universidade Federal Rural do Semi-Árido, Mossoró, RN, Brazil.

Microstrip antennas arrays are used to provide a required pattern that is difficult to be achieved with a single element feed [8]. The MSA array showed in [13] has 12.5 dBi and can provide long-range RFID communication, but they are costly and difficult to manufacture, due to its specificity and complexity, being also large and heavy in comparison with a single element microstrip antenna.

Another way to obtain a high-gain antenna is by using a single element antenna configuration with a metamaterial superstrate acting as a planar lens [14, 15]. Metamaterials (MTM) are dispersive artificial electromagnetic media with physical properties engineered by assembling periodically structures, called unit cells, much smaller than the wavelength of the impinging electromagnetic wave [16, 17]. Negative refractive index metamaterials (NIM) are engineered materials with a negative refractive index that, among other things, can be used as a superstrate of a microstrip antenna and acts as a convergent planar lens, focusing electromagnetic waves and thus enhancing the maximum gain of antennas [18, 19]. This configuration provides a low-cost, easy to manufacture, small, light and flexible antenna, that could operate as general-purpose circular polarized microstrip antenna, or as a gain-enhanced antenna for long-range RFID applications when used in combination with a novel metamaterial superstrate acting as a planar lens. This approach to achieving gain enhancement has already been used for several communication systems for a wide range of operating frequencies bands, like S, C and X bands [15, 19–21], but never used for in UHF RFID Readers antennas operating at 902–928 MHz frequency band.

Therefore, it is in that context that comes the idea to develop a novel general-purpose single element MSA that can be used in short and medium range communications for RFID applications [6, 7], an also novel NIM superstrate acting as a planar focusing lens, and the combination of both, forming a novel, light, small, low-cost, gain-enhanced antenna for long-range RFID applications [4, 5], using the 902–928 MHz frequency band. This development contributes to reducing the expensive costs of the needed infrastructure [22], pushing the RFID adoption in a wide range of applications globally. This work also provides a fresh understanding of negative index metamaterial around 1GHz frequency band.

This paper continues describing the antenna design, including the general-purpose MSA, NIM superstrate, and the entire radiation set assembled together. Then, the experimental and simulation results are shown, analyzed and discussed. A set of parametrical studies are done to understand the design of the superstrate metamaterial and its combination with the general-purpose MSA, forming thus the MSA with NIM planar lens. Finally, the conclusion of this paper is presented, synthesizing the most significant achievements of this work.

2. ANTENNA CONCEPTION

The conception of this low-cost gain-enhanced MSA with NIM planar lens for long-range RFID applications begins with the design of the general-purpose MSA and the NIM planar lens. Then, both are bundled together to compose the final configuration of this MSA with NIM planar lens. Finally, the entire set is manufactured for validation.

The first step in the general-purpose MSA design is the definition of its constitutive matter. This antenna design considers the use of galvanized steel sheets with $tg = 0.3$ mm of thickness, cylindrical polypropylene spacers with 3 mm radius and a pigtail made of RG-316 cable and a TNC-RP female connector, emphasizing the low-cost nature of this MSA.

After that, it is time to focus on the electromagnetic engineering of it. The square patch is the most straightforward structure to manufacture and analyze [8], being used from the simplest to the most demanding applications. Two stacked patches, a main and a parasite, is a compact structure to provide a substantial impedance bandwidth [10]. Circular polarization is relevant to several RFID applications due to their difficulty to determine the relative orientation between reader and tag antennas [12]. The use of a T-junction is a simple and cheap way to excite two resonant, orthogonal and quasi-degenerate modes, TM_x001 and TM_x010, needed to make the antenna radiation to be circularly polarized [9]. A tapered three-dimensional transition is a compact impedance matching structure that connects the feeding network to the square patch [9]. Thus, this general purpose MSA is based on [23] and specified as circularly polarized microstrip square patch with a ground plane, a main and a parasite patches, a microstrip feed line working as a T-junction and a three-dimensional transition impedance matching device that binds the main patch with the feeding network mentioned above. The ground plane is separated from the main patch by four cylindrical polypropylene spacers with *hpi* of height that provide

an air substrate layer which reduces losses, such as those from surface waves, increasing thus bandwidth, efficiency, and gain, for instance [11]. The use of this air substrate layer is the most significant structural advance of this general-purpose MSA in comparison with [23]. The parasite square patch is on top of the main, being also separated by four cylindrical polypropylene spacers with *hpa* of height and another air substrate layer. The proposed configuration for the general-purpose RFID reader MSA can be seen in Fig. 1.

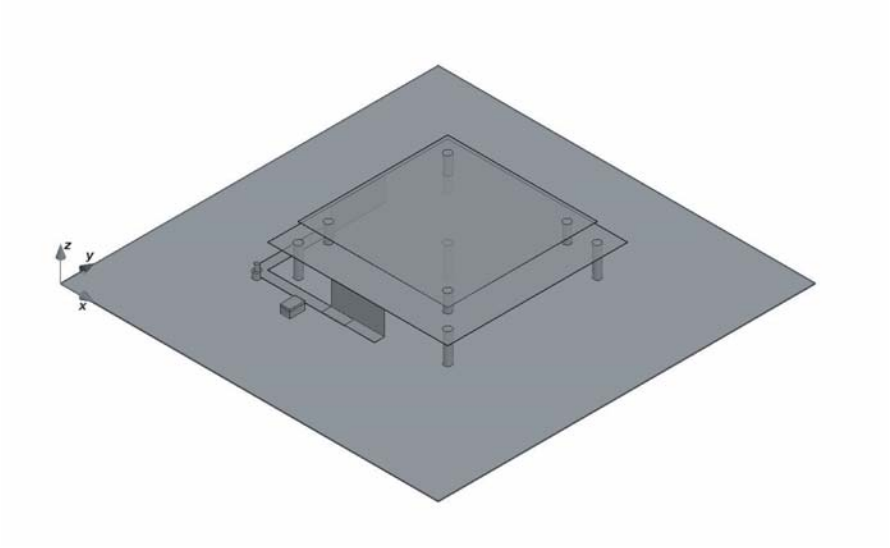

Figure 1. Proposed general-purpose MSA configuration.

The exact dimensions of the antenna configuration are illustrated in Fig. 2, being determined using the systematic design method defined in [24] in conjunction with the mathematical and physical tools shown in [8–12] and several parametric studies made with Ansoft HFSS^{TM}.

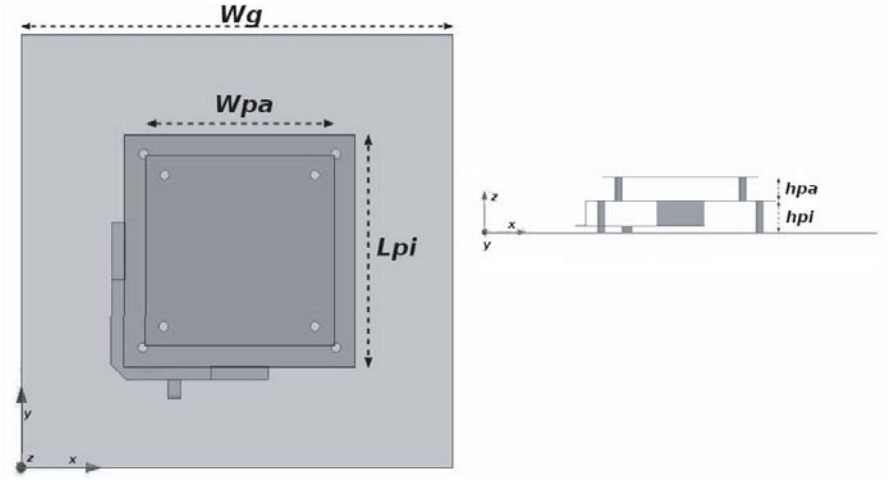

Figure 2. Top and side view of general-purpose MSA configuration.

Table 1 exhibits numeric values of the antenna most relevant dimensions.

After the design of the general-purpose MSA, the NIM planar lens is then designed. This process also starts with the selection of the material used in this NIM planar lens fabrication, being it based on $td = 1.6\,\text{mm}$ thickness FR4 sheets, with $tc = 0.140\,\text{mm}$ of thickness copper conductor. Naturally, the geometry selection of the metamaterial unit cell is the next step. Jerusalem Cross (JC) is a geometry based on a pair of I-shaped crossed dipoles that are used in several metasurfaces [25–27]. Unit cells based

Table 1. General-purpose MSA parameters.

Parameter	Wg	Lpi	Wpa	hpi	hpa
Length	250 mm	124 mm	95 mm	20 mm	12 mm

on tightly coupled JC conductor pairs, as seen in [16, 28, 29], produces metamaterials able to support both symmetric (electric) and antisymmetric (magnetic) resonance modes whose superposition leads to and effective NIM media. This Jerusalem Cross Pair (JCP) metamaterial is easy to manufacture and can provide an effective negative refractive index response with a small sensibility to polarization and incidence angle of the incoming plane wave, simplifying the design and fabrication process [16, 28]. Basically, the design process of this infinite periodicity JCP/NIM slab is guided knowing that the capacitance of this metamaterial came from the electric field present in the gaps between each unit cell, the inductance is related to the electric current flowing in the body of the I-shaped dipole, and thicker substrates results in broader bandwidths [25–30]. Though, the NIM unit cell has two sheets of FR4 separated by a thick air substrate layer, providing enough negative refractive bandwidth. The copper Jerusalem Crosses are present in the outer faces of each FR4 sheet. This NIM unit cell configuration is illustrated in Fig. 3.

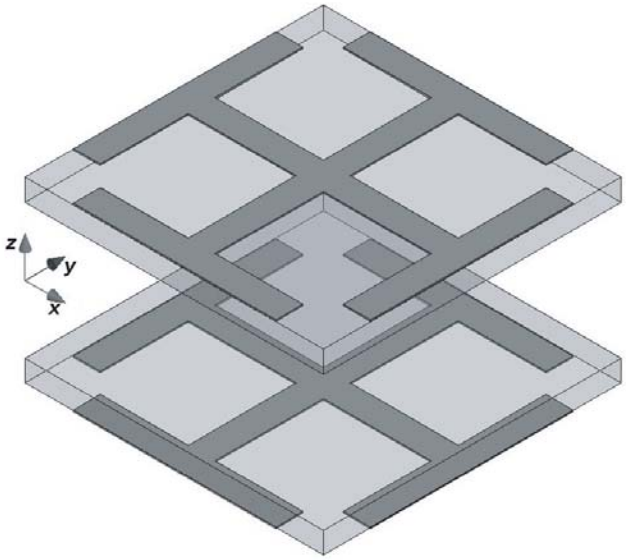

Figure 3. NIM unit cell configuration.

The exact dimensions of the NIM unit cell are obtained using Ansoft HFSS^{TM} master and slave periodic boundary conditions and flouquet port excitation, which emulates a NIM slab with infinite repetitions of unit cells, allowing the elaboration of multiple parametric studies, which can be seen in Section 4. Fig. 4 presents the most critical dimensions of NIM unit cell.

Table 2 exhibits the numeric values of NIM unit cell most relevant dimensions.

Table 2. Important NIM unit cell parameters.

Parameter	Wt	Wc	Lm	Lit	g	hm
Length	15 mm	2 mm	22.10 mm	18 mm	0.05 mm	13.20 mm

To conclude the design of this gain-enhanced MSA for long-range RFID applications, the NIM planar lens must have its dimensions defined and then bundled with the general-purpose MSA. For

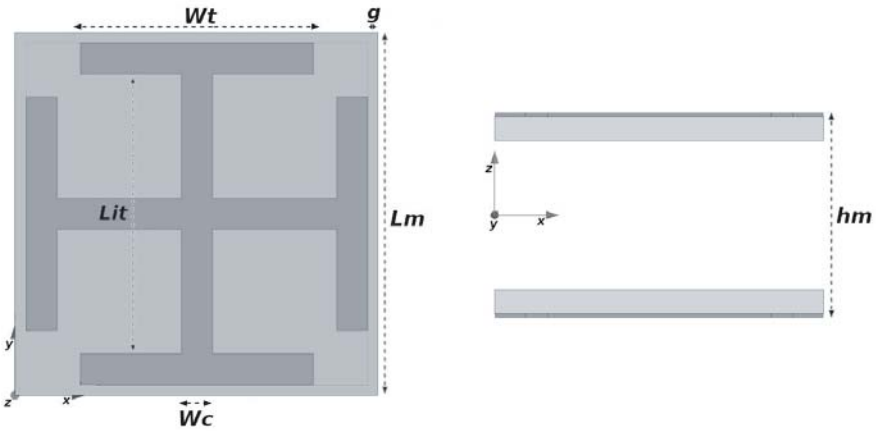

Figure 4. Top/bottom and side view of the NIM unit cell.

that matter, the parametric studies presented in Section 4 are used to find the optimal value for the size of the metamaterial unit cell array and its height above the general-purpose MSA parasite patch. The design process resulted in a NIM planar lens with 5×5 metamaterial unit cell array attached to mechanical support that allows an easy coupling between the general purpose MSA and the NIM planar lens. The support is made of an acrylic (polymethyl methacrylate) slab and four cylindrical polypropylene spacers. The configuration of the NIM planar lens with its support is shown in Fig. 5.

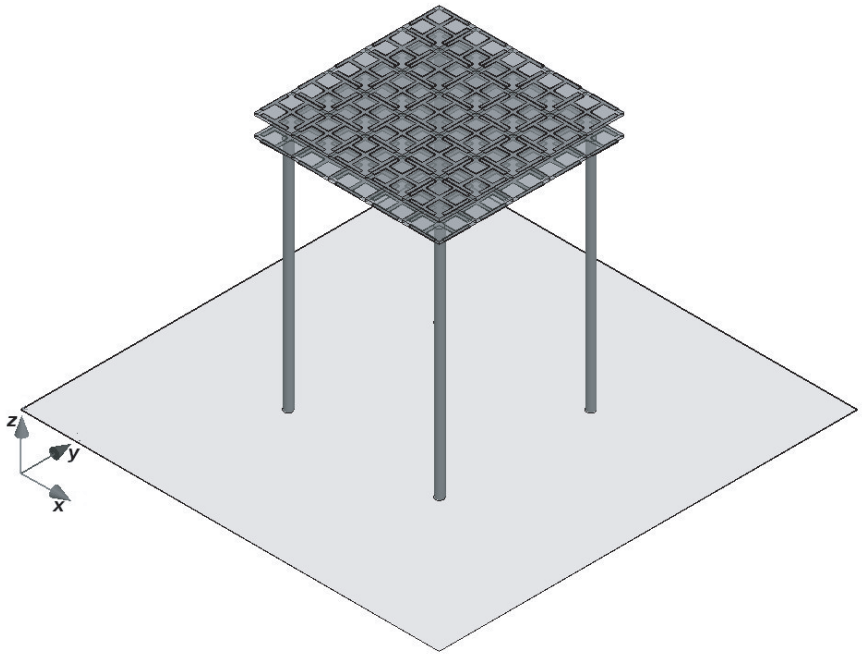

Figure 5. NIM planar lens with support configuration.

In Fig. 6, the exact dimensions of the NIM planar lens and its support are illustrated.

Table 3 exhibits the most relevant dimensions of the NIM slab and its support.'

Finally, the general-purpose MSA is coupled easily to the support of the NIM planar lens using four polypropylene cylindrical spacers of 32 mm of height, forming the low-cost gain-enhanced antenna with NIM planar lens for long-range UHF RFID applications. This device configuration is presented in Fig. 7.

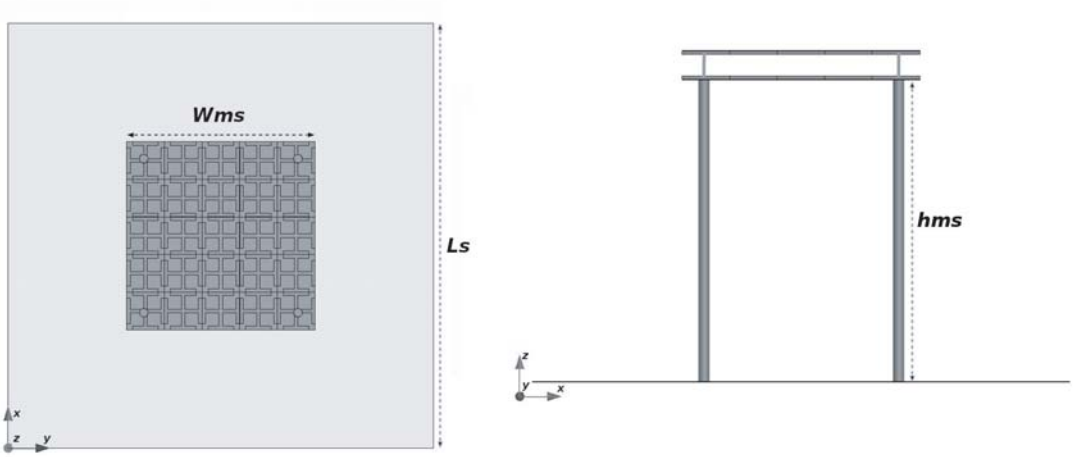

Figure 6. Top and side view of NIM planar lens with support.

Table 3. Important NIM slab and its support parameters.

Parameter	Ls	Wms	hms
Length	250 mm	110.50 mm	140 mm

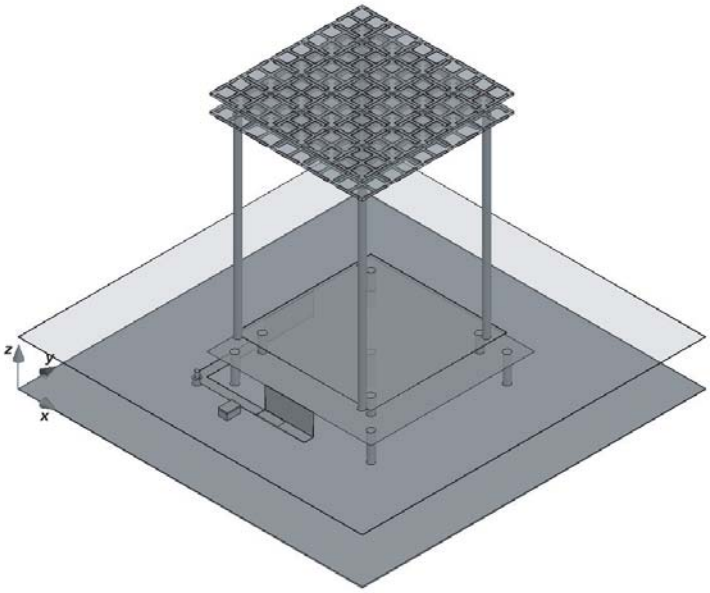

Figure 7. MSA with NIM planar lens configuration.

Now, with the general-purpose antenna, the NIM planar lens and its combination, the novel gain-enhanced MSA with NIM planar lens, designed, they are manufactured using those previously specified materials such as galvanized steel sheets, FR4 slabs, and polypropylene cylindrical spacers. Fig. 8(a) shows the prototype of the general-purpose MSA. The prototype of the NIM planar lens with its mechanical support is seen in Fig. 8(b).

The prototype of the low-cost gain-enhanced antenna with metamaterial planar lens for long-range UHF RFID applications operating at the ITU Region 2 frequency band, 902–928 MHz, is viewed in Fig. 9.

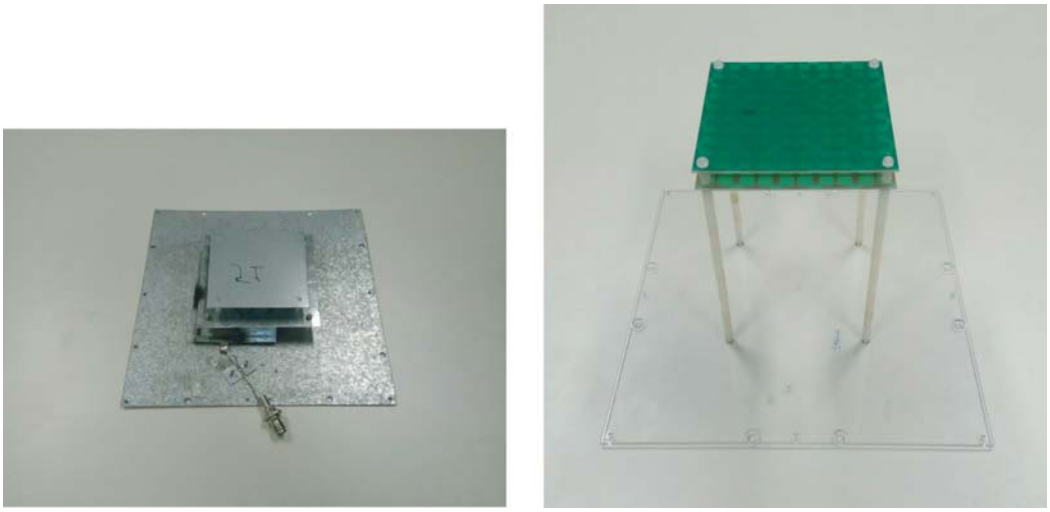

(a) (b)

Figure 8. Fabricated prototypes. (a) General-purpose MSA and (b) NIM planar lens with support.

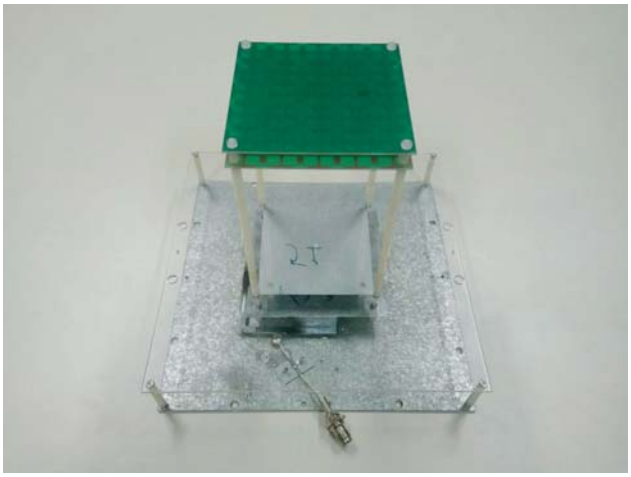

Figure 9. MSA with NIM planar lens fabricated prototype.

3. RESULTS AND DISCUSSION

The NIM planar lens, general-purpose MSA, and gain-enhanced MSA with NIM planar lens are validated by simulated and/or experimental results of transmission and reflection coefficients (S-parameters), effective electric permittivity, magnetic permeability, refractive index, and wave impedance, for the metamaterial, and gain, axial ratio, reflection coefficient, and read range, for both antennas. The simulations, as mentioned earlier, were made with Ansoft HFSS^{TM} and GNU Octave. Experimentally measured result of those devices for impedance, far-field and read range characterization were obtained using an Agilent 8510C network analyzer, EMScan RFxpert RFX2 Antenna Performance Scanner, and a Honeywell IF2 Monostatic UHF RFID reader, a 4m LMR-195 cable and Avery Dennison AD-237 tags, respectively.

First, the simulated results regarding the metamaterial are presented. Figs. 10(a) and 10(b) show magnitude and phase of reflection and transmission coefficients of the NIM infinite slab based on the unit cell presented in Fig. 3. In Fig. 10(a), is possible to observe a transmission peak and reflection dip of 0.83 at 873 MHz and 0.21 at 876 MHz, respectively. A dip in the phase of the transmission coefficient

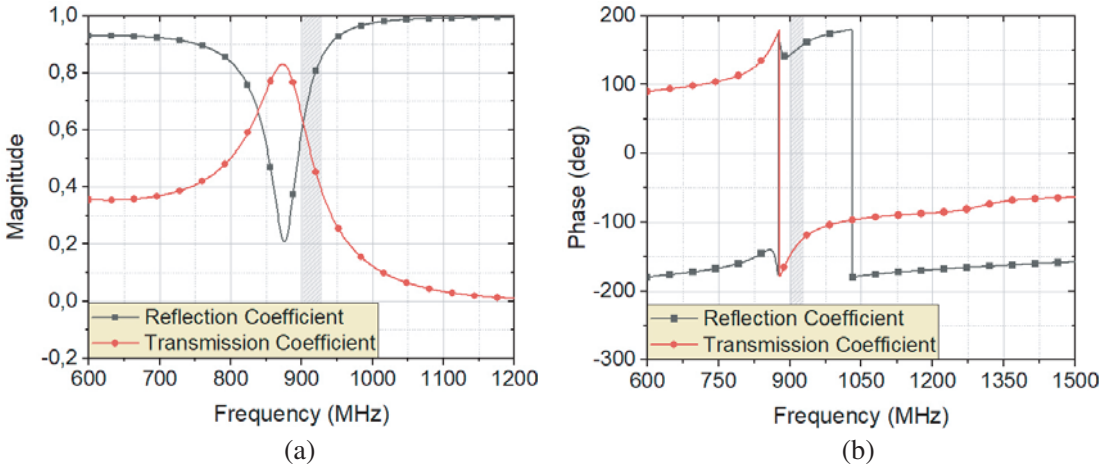

Figure 10. Reflection and transmission coefficient of the infinite periodicity JCP/NIM, (a) magnitude and (b) phase.

in 878 MHz can be seen in Fig. 10(b), indicating the existence of a negative index band. In this paper, the time-harmonic convention adopted is $e^{j\omega t}$.

The metamaterial parameters (impedance, effective refractive index, electric permittivity and magnetic permeability) were obtained using an algorithm for Octave based on the retrieval method specified in [31, 32] that uses the transmission and reflection coefficient. In Fig. 11(a), a negative refractive band can be seen in the 886–1326 MHz frequency interval, representing a 48% fractional band for 915 MHz and presenting a minimum value of −12.30 at 886 MHz. The wave impedance z of the slab is presented in Fig. 11(b) and is used in conjunction with the effective refractive index n to retrieve the permeability and the permittivity directly from $\varepsilon = z/n$ and $\mu = zn$.

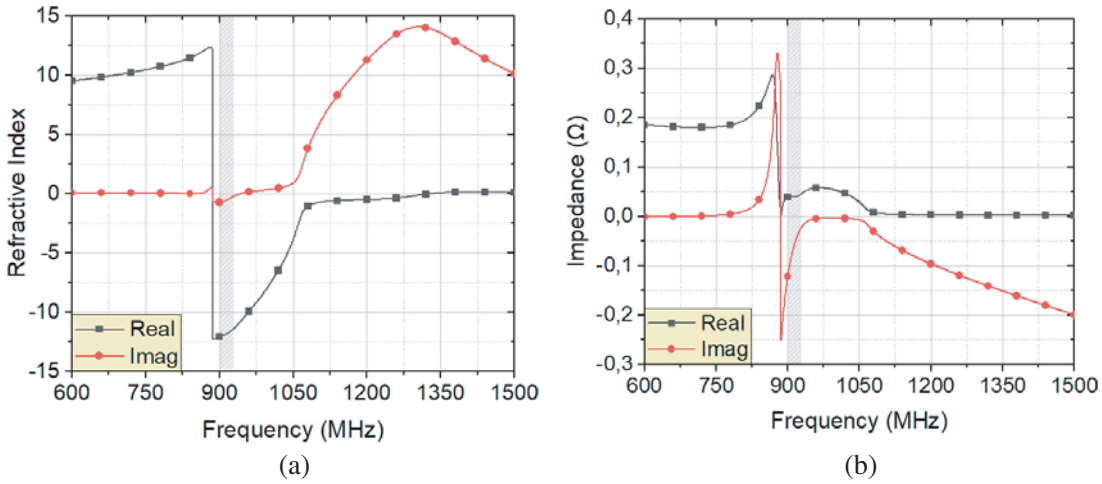

Figure 11. Extracted effective parameters of the infinite periodicity JCP/NIM, (a) refractive index and (b) impedance.

Fig. 12(a) shows a negative permittivity band defined by the 888–3406 MHz frequency interval, presenting a minimum value of −204.70 at 932 MHz. The negative permeability band of the NIM slab band is presented in Fig. 12(b) and defined by the 885–1065 MHz frequency interval, representing a 19.70% fractional band for 915 MHz and presenting a minimum value of −0.56 at 898 MHz.

The simulated and experimental values of the reflection coefficient for both antennas can be observed

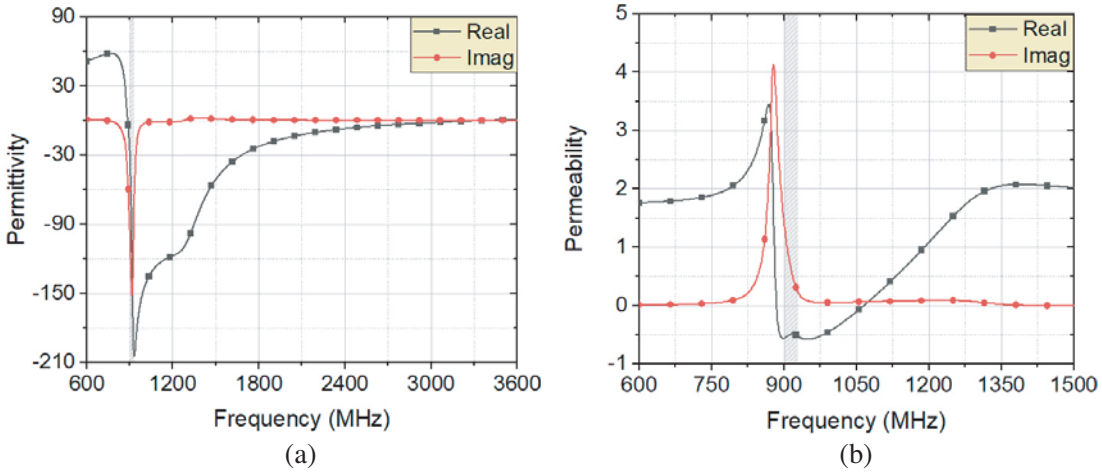

Figure 12. Extracted effective parameters of the infinite periodicity JCP/NIM, (a) permittivity and (b) permeability.

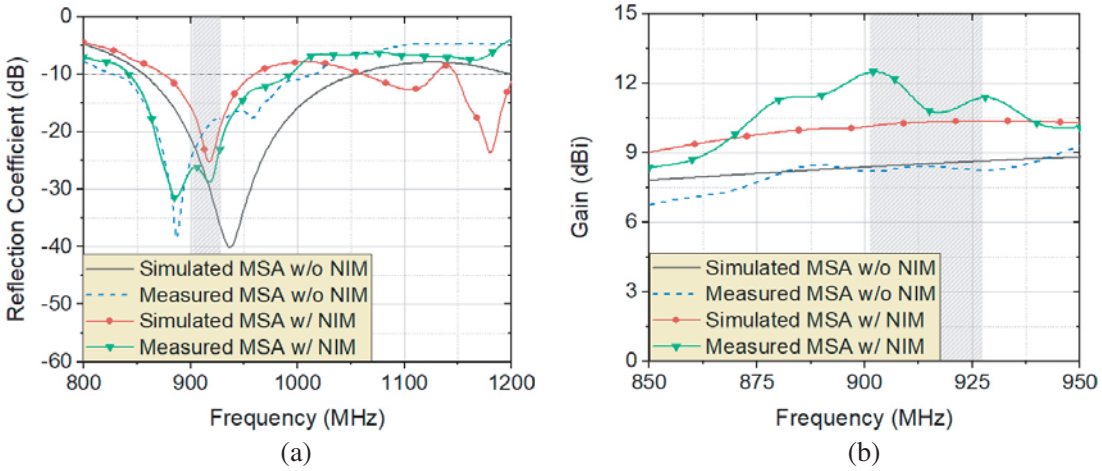

Figure 13. Measured and simulated values of the MSA with NIM planar lens and general-purpose MSA, (a) reflection coefficient and (b) gain at broadside.

in Fig. 13(a). The general purpose MSA presents a −10 dB impedance band of 828–1015 MHz with 187 MHz (20.49%) of width. The MSA with a NIM planar lens reflection coefficient shows a −10 dB impedance band of 843–993 MHz with 150 MHz (16.44%) of width. Those experimentally measured results are similar to the simulation.

The broadside gain of both antennas is seen in Fig. 13(b). In the 902–928 MHz frequency band, the general purpose MSA presents a maximum broadside gain of 8.43 dBi at 915 MHz and the MSA with NIM planar lens performed 12.50 dBi at 902 MHz. Furthermore, those results are clear evidence that superstrate works well as a NIM planar lens in this frequency band.

The simulated and experimental radiation patterns of both RF devices in x-z and y-z planes are illustrated in Fig. 14 for 915 MHz RFID central frequency. The maximum experimentally measured gain in both planes are of 8.43 dBi for general-purpose MSA, and of 10.82 dBi for the MSA with a NIM planar lens.

Figures 13(b) and 14 present a slight discrepancy between simulation and measured results regarding the gain of both antennas. Several reasons can justify that. The first one is related to limitations and difficulties of the RFxpert very-near-field measurement system, especially when dealing with large antennas like the MSA with NIM planar lens, as can be seen in [33, 34]. The second one is

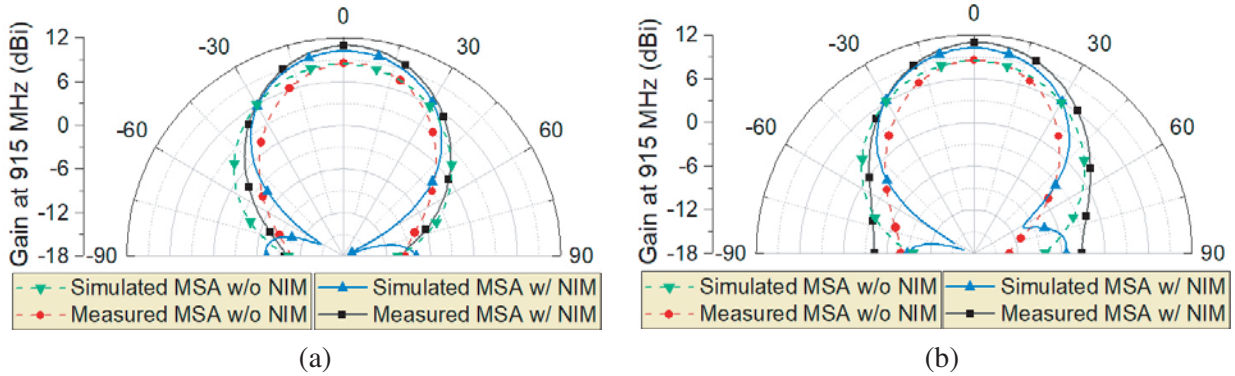

Figure 14. Measured and simulated radiation patterns of the MSA with NIM planar lens and general-purpose MSA at 915 MHz, (a) x-z plane and (b) y-z plane.

related to deviations between specified and actual values of the FR4 substrate dielectric constant and tangent loss. The third one regards possible errors in the copper JC fabrication on the FR4 substrate layer and in the assembly of two of those together to form the NIM planar lens. The last one is associated with a flawed combination of the general-purpose MSA with NIM planar lens to form the MSA with NIM planar lens.

Regarding axial ratio, the general-purpose MSA presented a 3 dB bandwidth of 35 MHz placed at 896–931 MHz with minimum values of 0.1 dB at 916.20 MHz. Nevertheless, the MSA with a NIM planar lens presented only elliptical polarization with a minimum of 6.9 dB at 896 MHz. The axial ratio of 7.30 dB at 913.10 MHz is the minimum in the 902–928 MHz frequency band. Fig. 15 shows the simulated and measured axial ratio values for both antennas.

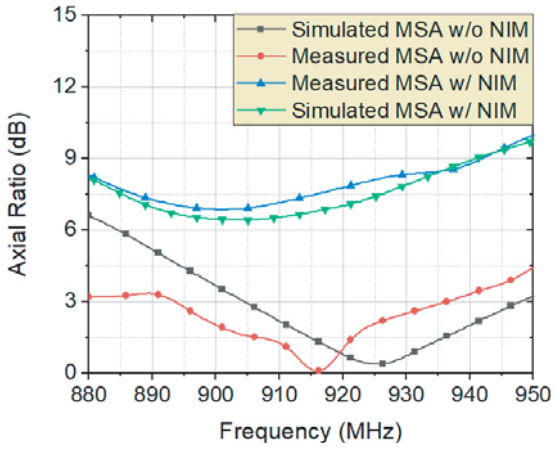

Figure 15. Measured and simulated axial ratio values of the MSA with NIM planar lens and general-purpose MSA.

The general purpose MSA and the MSA with NIM planar lens were submitted to the read range tests adapted from [2, 13, 35]. Separately, each antenna prototype is connected to the IF2 RFID Reader using a 4 m LMR-195 and fixed 1 m above the ground with their broadside aligned to an AD-237 tag. In Fig. 16, an illustration of the read range test scenario can be seen adapted from [35]. The maximum read range d were first obtained with an AD-237 tag placed horizontally and then, vertically. The output power used was of 30 dBm in all tests.

Table 4 summarizes the results of the read range tests. The MSA with NIM planar lens read tags at a greater distance, considering both tag orientations. The general purpose MSA presented the

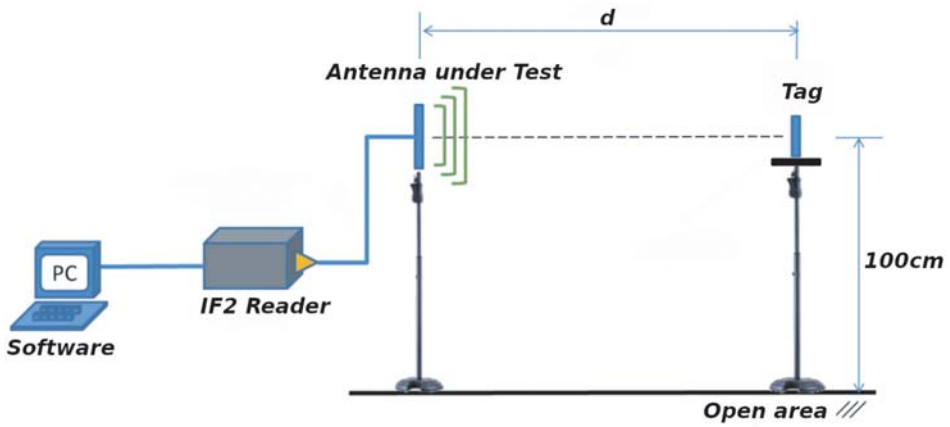

Figure 16. Read range tests scenario.

Table 4. Read range tests results.

Antenna	Tag Orientation	Read Range (d)
Genaral Purpose MSA	Horizontal	14.50 m
	Vertical	11.50 m
MSA with NIM planar lens	Horizontal	17.50 m
	Vertical	9 m

smaller difference between read range for each tag orientation. This test results validate the use of both antennas in the communication system that they are designed for and reinforce the gain enhancement and axial ratio degradation in MSA with NIM planar lens in comparison with general-purpose MSA.

Finally, a comparison between the general-purpose MSA, the MSA with NIM planar lens, and other two antennas for UHF RFID operating at 902–928 MHz frequency band can be seen in Table 5. Unfortunately, no other antenna with NIM planar lens for ISO 18000-6c UHF RFID systems were found to integrate this comparison.

Table 5. Comparison between this work and other UHF RFID reader antennas.

Parameter	General Purpose MSA	MSA from [10]	MSA with NIM Planar Lens	MSA Array from [13]
Bandwidth (Z)	828–1015 MHz	740–970 MHz	843–993 MHz	759–1026 MHz
Bandwidth (AR)	896–931 MHz	818–964 MHz	Elliptical	828–993 MHz
Maximum Gain	8.43 dBi	$\cong$ 9 dBi	12.50 dBi	12.50 dBi
Fabrication Complexity	Low	Medium	Medium	High
Ground plane area	625 cm^2	625 cm^2	625 cm^2	1936 cm^2
Volume	2187 cm^3	2187 cm^3	3871 cm^3	4388 cm^3
Weight	352 g	Unknown	648 g	$\cong$1160 g
Communication Range in RFID	Medium (Extensible to Long)	Medium	Long	Long

4. PARAMETRIC STUDIES

Parametric studies were used to investigate the influence of the design parameters of the general-purpose MSA, the NIM planar lens and the combination of both, the gain-enhanced MSA with a NIM planar lens, on their characteristics and performances, providing crucial information for their design and optimization.

The general-purpose MSA is constructed under well-established knowledge [8–11]. The effects under the majority of the antenna parameters are already well known, and thus they are not shown in this paper since it is only used for optimization.

In [16, 28, 29], parametric studies about the JCP Metamaterial provide some meaningful analysis considering it an infinite array of unit cells, but both are focused only in transmission and reflection coefficient in frequencies above 5 GHz. The studies shown in this paper observes the influence of the most critical design dimensions Wt, Lit, g and hm in reflection and transmission coefficient and in effective permittivity, permeability and refractive index, focusing on the frequencies around UHF RFID 902–928 MHz frequency band.

Finally, the combination of the NIM planar lens and the general-purpose MSA to form the MSA with NIM planar lens is studied observing the influence of the number of unity cells on NIM planar lens and its height, hms, above the parasitic patch on the gain and the reflection coefficient of the

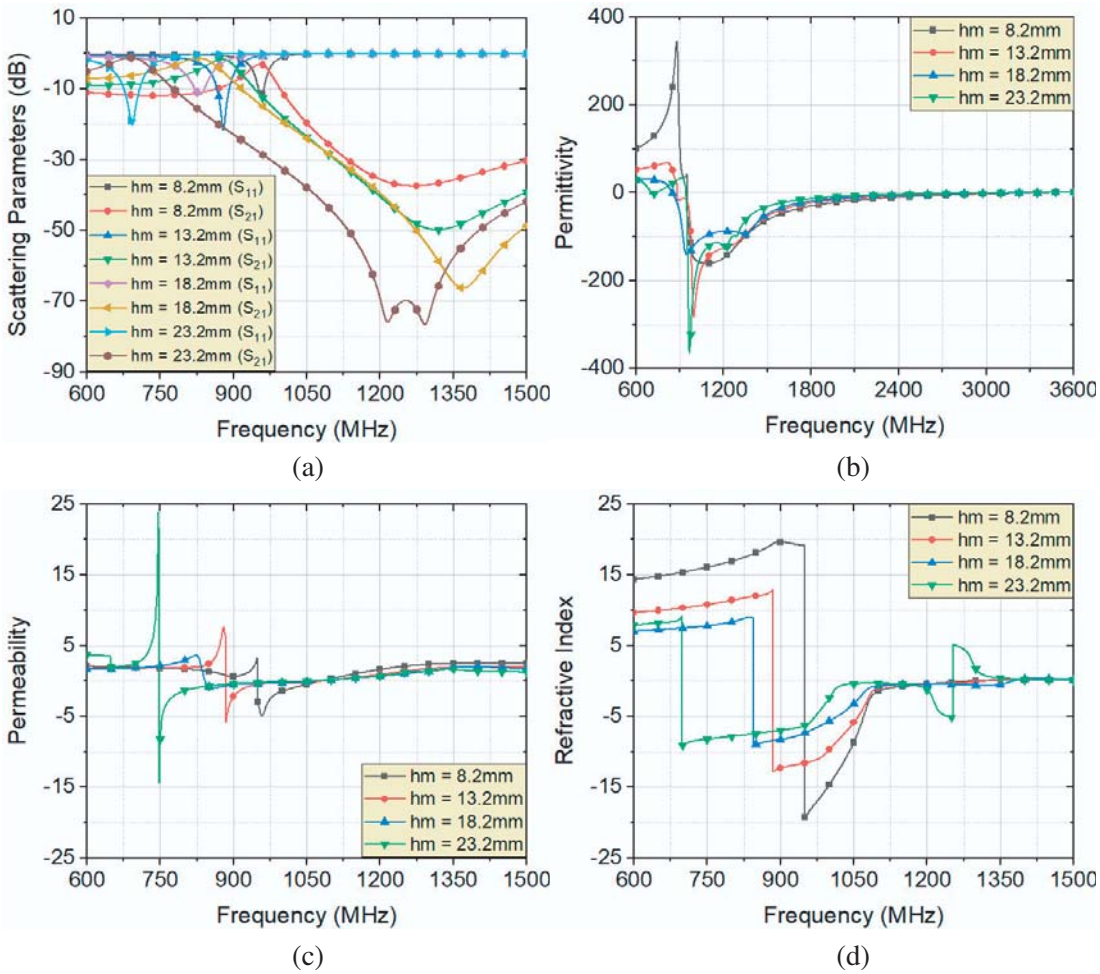

Figure 17. Constitutive and scattering parameters of the infinite periodicity JCP/NIM at different hm values, (a) reflection and transmission coefficient, (b) real part of effective permittivity, (c) real part of effective permeability and real part of effective refractive index.

antenna. This study provides a novel understanding of the use of a NIM planar lens approach for gain enhancement around 1 GHz.

The parametric studies are based on simulated results due to the good agreement between them and that experimentally obtained. In order to provide a clearer understanding of the influence between the design parameters and the desired characteristics of the metamaterial and the MSA with NIM planar lens, only one parameter at a time is varied, while others are kept unchanged. The design parameters of the unity cell for the parametric studies are: $Wt = 15$ mm, $Wc = 2$ mm, $Lm = 22.10$ mm, $Lit = 18$ mm, $g = 0.05$ mm, $hm = 13.20$ mm and $tc = 0.14$ mm. For the MSA with NIM planar lens, the design parameters are: $Wg = 250$ mm, $Lpi = 124$ mm, $Wpa = 95$ mm, $hpa = 20$ mm, $hpi = 12$ mm, $Ls = 250$ mm, $Wms = 110.50$ mm and $hms = 140$ mm.

4.1. The Effects on JCP Metamaterial

As shown in Fig. 4, the most critical parameters related to the JCP/NIM electromagnetic characteristics are the length of I-shaped dipole, Lit, the width of its tip, Wt, the height of the air layer between FR4 sheets, hm, and the gap between the tip of the dipole and the edge of the FR4 dielectric, g.

Figure 17 shows the impact of hm variation on reflection and transmission coefficient, and on effective permittivity, permeability and refractive index. The increase in hm practically maintains the negative effective permittivity band in the same frequency interval and with similar width. The other

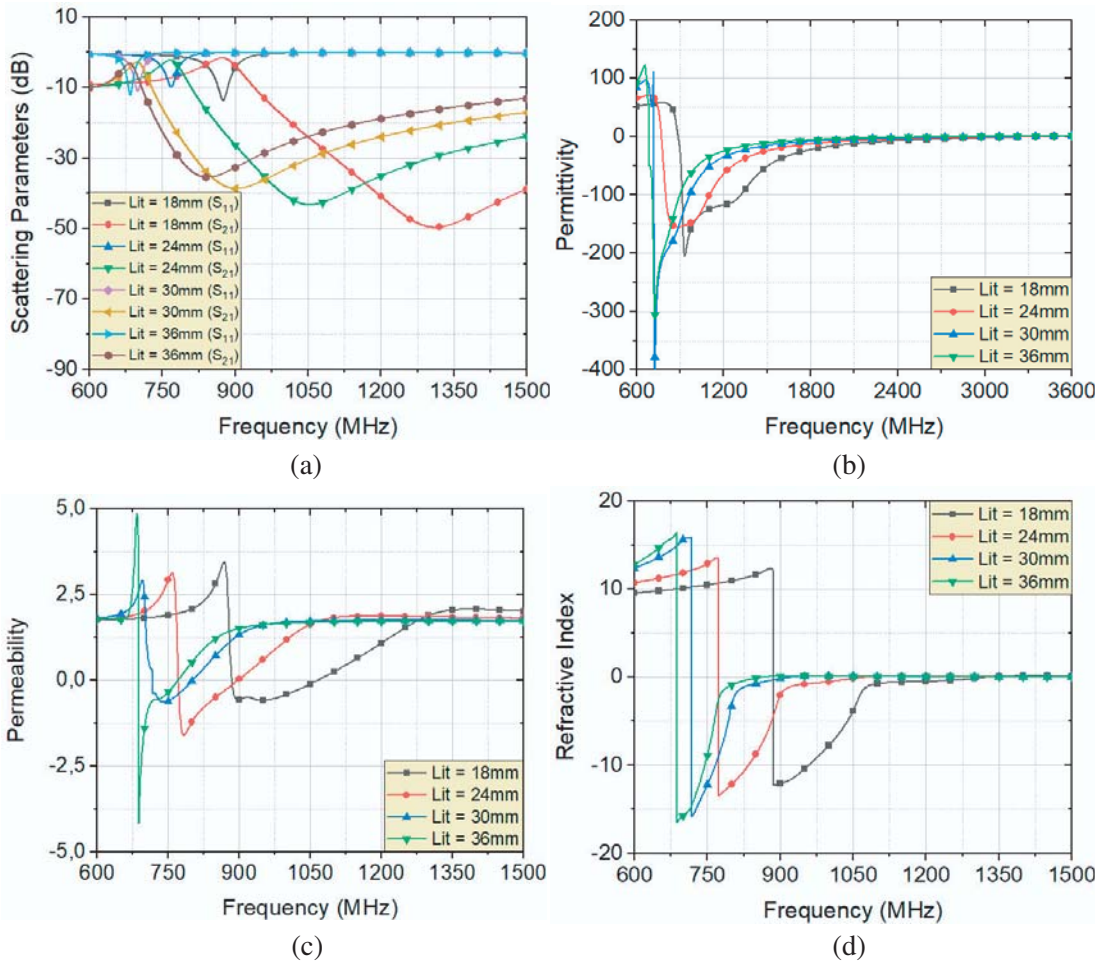

Figure 18. Constitutive and scattering parameters of the infinite periodicity JCP/NIM at different Lit values, (a) reflection and transmission coefficient, (b) real part of effective permittivity, (c) real part of effective permeability, and real part of effective refractive index.

three bands are all shifted down, with significative enlargement in their widths.

Figure 18 presents the effects of *Lit* variation on reflection and transmission coefficients, and on effective permittivity, permeability, and refractive index. The increment in *Lit* offsets down all five bands, narrowing their widths. The refractive effect intensity increases due to the tuning among permeability and permittivity frequency bands.

Figure 19 illustrates the influence of g variation on reflection and transmission coefficients, and on effective permittivity, permeability, and refractive index. The increment in g moves the negative effective permittivity band up, but its width is diminished. The other four bands are all enlarged and pushed up in the frequency spectrum.

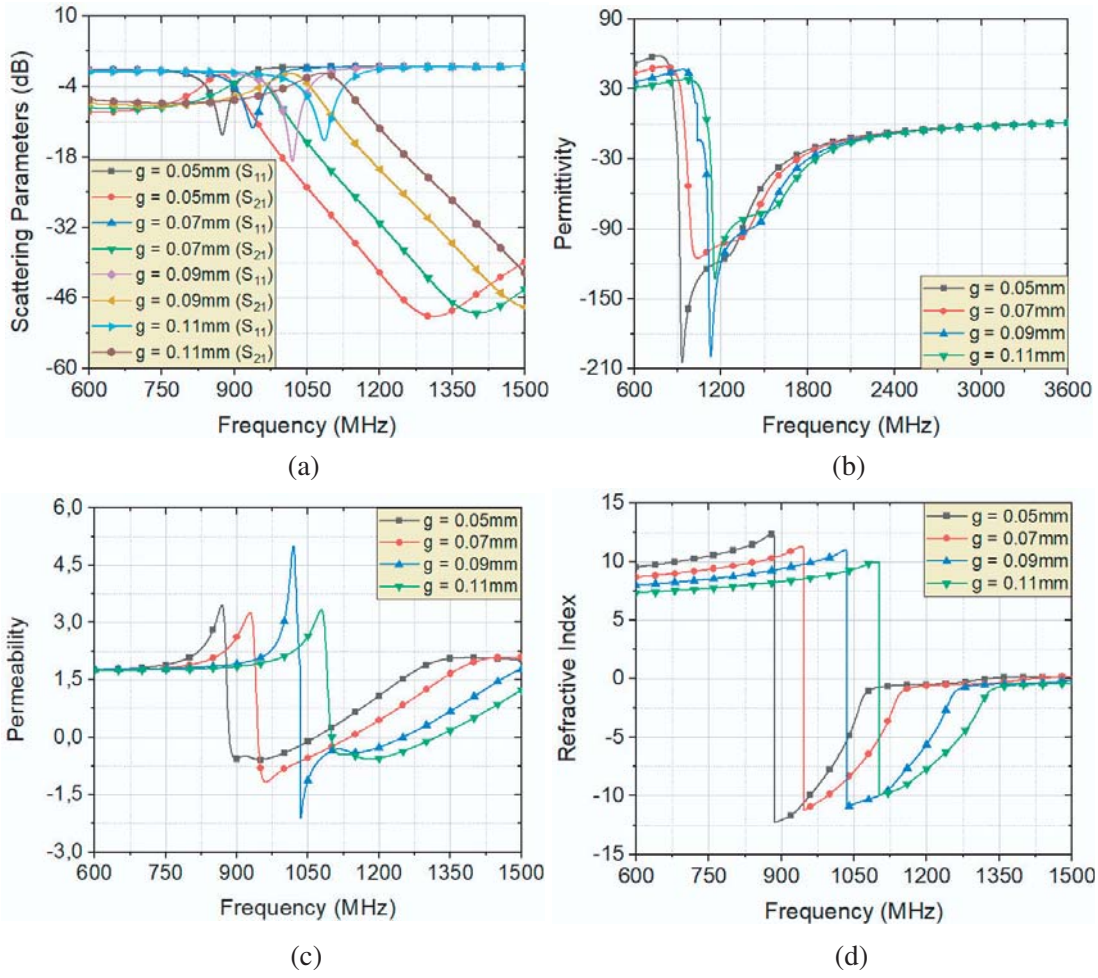

Figure 19. Constitutive and scattering parameters of the infinite periodicity JCP/NIM at different g values, (a) reflection and transmission coefficient, (b) real part of effective permittivity, (c) real part of effective permeability, and real part of effective refractive index.

Figure 20 shows the effects of Wt variation on reflection and transmission coefficients, and on effective permittivity, permeability, and refractive index. The increment in Wt provides an enlargement in reflection and transmission coefficient bandwidths initially. Then, that tendency is reversed, and it starts to narrow down. The mentioned frequency bands are also moved down during Wt increase. The other three bands are all diminished and moved down in the frequency spectrum.

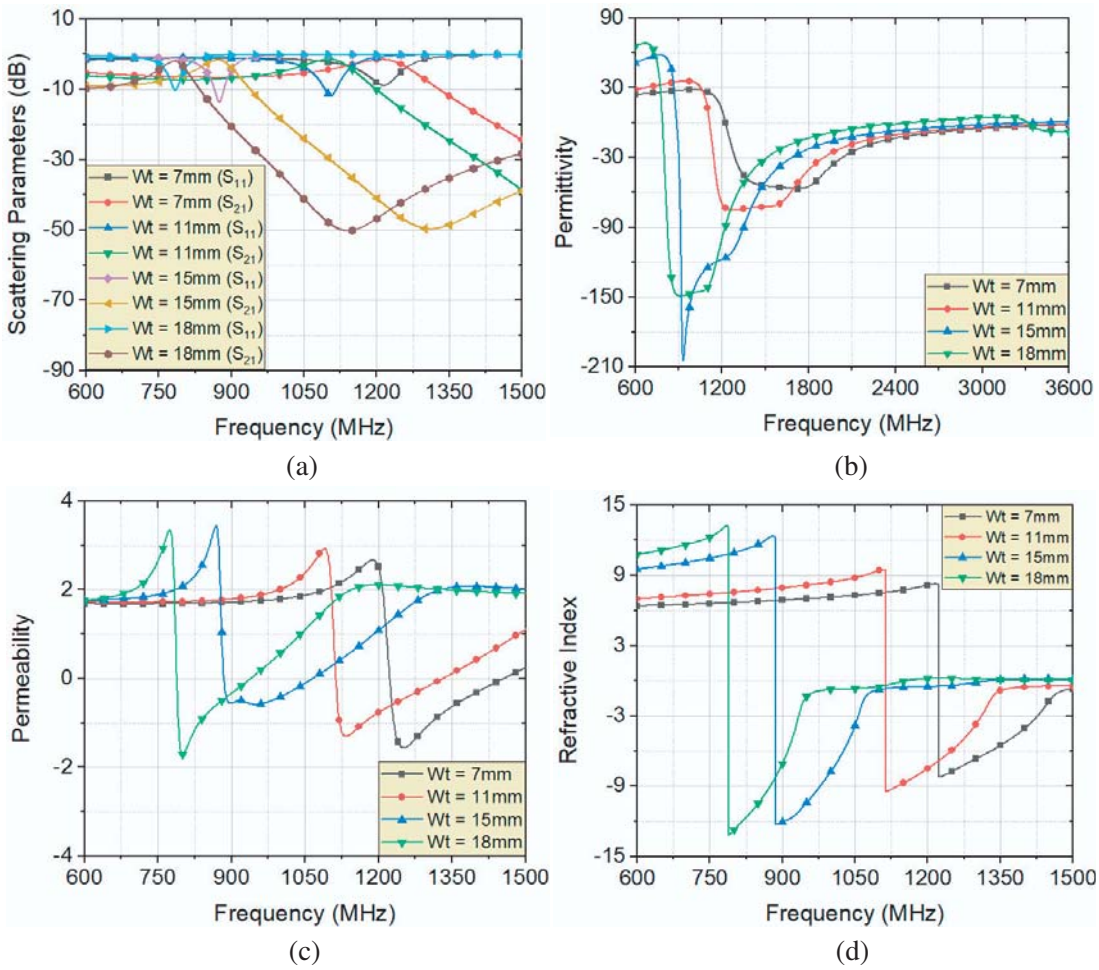

Figure 20. Constitutive and scattering parameters of the infinite periodicity JCP/NIM at different Wt values, (a) reflection and transmission coefficient, (b) real part of effective permittivity, (c) real part of effective permeability, and real part of effective refractive index.

4.2. The Effects on MSA with NIM Planar Lens

As seen in Fig. 5, to form the MSA with NIM planar lens as a combination of the NIM slab and general-purpose MSA, the number of unity cells of the NIM planar lens and its height, hms, above parasitic patch must be determined. The antenna gain and reflection coefficient are the parameters observed in those studies, trying to maximize gain and maintain the 902–928 MHz frequency band contained in the impedance band of the antenna.

Fig. 21 shows the gain and reflection coefficient for the variation in the number of unit cells. The gain of the MSA with NIM planar lens grow from 2×2 to a 6×6 unit cells array configuration, reaching its maximum value with 5×5 setup. The reflection coefficient is not significantly altered, maintaining the 902–928 MHz band covered.

Fig. 22 shows the gain and reflection coefficient for the variation of the height, hms, of the NIM planar lens with 5×5 unity cells array configuration. The gain of the MSA with NIM planar lens increase from 20 mm to 180 mm, reaching its maximum value at 140 mm. The reflection coefficient is severely altered in low values of hms, being this phenomenon caused by an intense coupling between the general-purpose MSA and the NIM planar lens. Even with this alteration, the 902–928 MHz band is still covered in $hms = 140$ mm configuration.

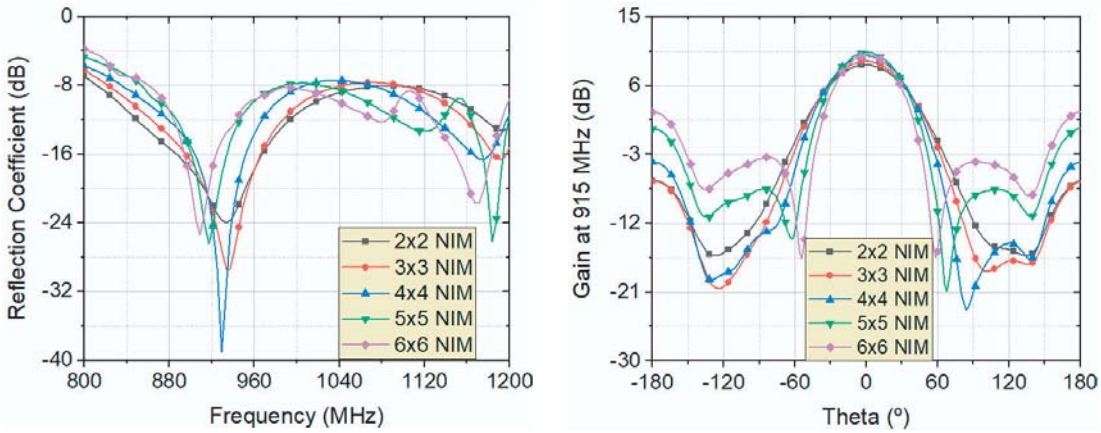

(a) (b)

Figure 21. (a) Reflection coefficient and (b) gain simulated values for the MSA with NIM planar lens with different number of unity cells in the metamaterial.

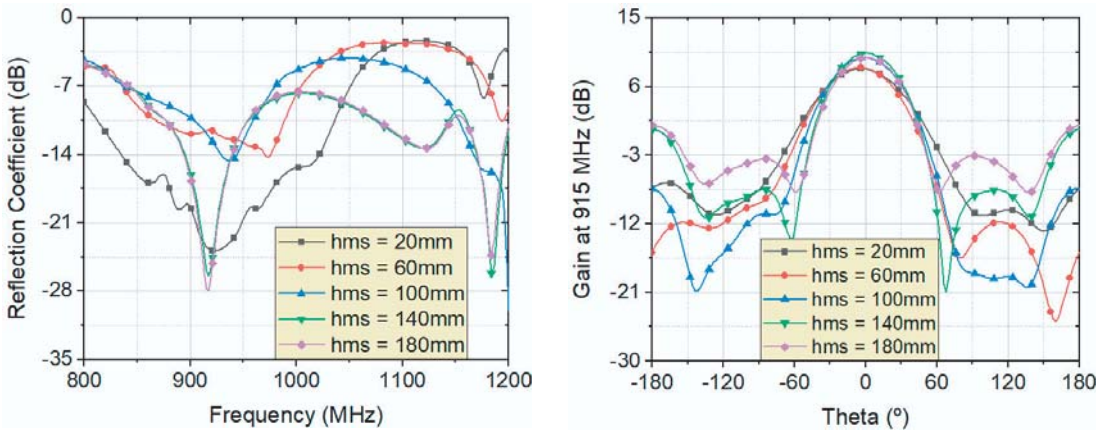

(a) (b)

Figure 22. (a) Reflection coefficient and (b) gain simulated values for the MSA with NIM planar lens with different *hms* values.

5. CONCLUSION

A novel low-cost gain-enhanced antenna with a NIM planar lens for long-range UHF RFID applications operating at 902–928 MHz frequency band is proposed in this paper. This device emerges as a conjunction of a general-purpose MSA and a NIM planar lens. The general-purpose MSA has an impedance and an axial ratio frequency band of 828–1015 MHz and 896–931 MHz, respectively, and a maximum gain of 8.43 dBi at 915 MHz. This device is low-cost, light, easy to manufacture, being thus an efficient well-rounded antenna that can be used in several short and medium-range UHF RFID applications.

The JCP/NIM planar lens has effective negative permittivity, permeability, and refractive index bands of 888–3406 MHz, 885–1065 MHz, and 886–1326 MHz, respectively, covering thus the entire 902–928 MHz frequency band.

The MSA with NIM planar lens has a maximum gain of 12.5 dBi, at 902 MHz, a 48.27% increase over the general-purpose MSA, an impedance frequency band of 843–993 MHz, and elliptical polarization. This device is light, compact, and easy to manufacture, inheriting from the general-purpose MSA several scalability advantages that reinforce the low-cost nature of this high-gain antenna. The attested gain

enhancement of this antenna in simulated and experimentally measured results confirms the effectiveness of the metamaterial as a planar lens.

Reading-range measurements tested the use of both antennas in a UHF RFID system operating at 902–928 MHz frequency band. This test result validates both antennas in their native communication system, ratifying the gain enhancement and axial ratio degradation in MSA with NIM planar lens in comparison with general-purpose MSA.

Finally, two sets of novel parametric studies are presented. The first one relates the most critical design parameters of a JCP metamaterial with reflection and transmission coefficient and effective permittivity, permeability and refractive index. The last one is related to the MSA with NIM planar lens design and observes the influence of the number of unity cells on NIM planer lens and its height above the parasitic patch of the general-purpose MSA on the gain and the reflection coefficient of the antenna. Both studies will be constructive in the design and optimization of JCP metamaterials and NIM gain-enhanced antennas, especially for UHF RFID applications based on ISO-18000-6C air interface protocol.

ACKNOWLEDGMENT

The authors are grateful to Instituto Federal de Educação, Ciência e Tecnologia do Ceará — Brazil, Fundação Cearense de Apoio ao Desenvolvimento Científico e Tecnológico — Brazil (FUNCAP), Coordenação de Aperfeicoamento de Pessoal de Nível Superior — Brazil (CAPES) (Finance Code 001) and the US Air Force Office of Scientific Research (AFOSR) (FA9550-16-1-0127) for the financial support.

REFERENCES

1. Das, R., "RFID Forecasts, Players and Opportunities 2017–2027," IDTechEx, 2017, available: https://www.idtechex.com/research/reports/rfid-forecasts-players-and-opportunities-2017-2027-000546.asp.
2. Brown, D., *RFID Implementation*, McGraw-Hill, 2007.
3. Sanghera, P., *RFID + Study Guide and Practice Exam*, Syngress Publishing, Inc., 2007, ISBN 978-0-470-10764-5.
4. Dias, E. M., J. A. Tatto, and D. A. Swiatek, "The National Vehicle Identification System in Brazil as a tool for mobility improvement," *Proceedings of the 19th International Conference on Communications*, 247–251, Zakynthos Island, Greece, 2015.
5. Chang, Y. and T. K. Shih, "RFID-based intelligent parking management system with indoor positioning and dynamic tracking," *10th International Conference on Ubi-media Computing and Workshops*, Pattaya, Thailand, 2017.
6. Moreira, E. C., R. Freitas, A. Morais, and A. S. B. Sombra, "RFID in cashew nut industry," *2014 IEEE Brasil RFID*, 31–34, São Paulo, Brazil, 2014.
7. Bertolini, M., E. Bottani, G. Ferretti, A. Rizzi, and A. Volpi, "Experimental evaluation of business impacts of RFID in apparel and retail supply chain," *International Journal of RF Technologies*, Vol. 3, No. 4, 257–282, 2012.
8. Balanis, C. A., *Antenna Theory: Analysis and Design*, 3rd Edition, Jonh Wiley & Sons Inc., 2005.
9. Garg, R., P. Bhartia, I. Bahl, and A. Ittipiboon, *Microstrip Antenna Design Handbook*, Artech House Inc., 2001.
10. Chen, Z. N., X. Qing, and H. L. Chung, "A universal UHF RFID reader antenna," *IEEE Transactions on Microwave Theory and Techniques*, Vol. 57, No. 5, 1275–1282, May 2009.
11. Chung, H. L., X. Qing, and Z. N. Chen, "A broadband circularly polarized stacked probe-fed patch antenna for UHF RFID applications," *International Journal of Antennas and Propagation*, Vol. 2007, Article ID 76793, 8 pages, 2007.

12. Dobkin, D., *RF in the RFID*, 1st Edition, Elsiveir Inc., 2008.
13. Hu, W., G. Wen, D. Inserra, Y. Huang, J. Li, and Z. D. Chen, "A circularly polarized antenna array with gain enhancement for long-range UHF RFID systems," *Electronics*, Vol. 8, No. 4, Article ID 400, 2019.
14. Ozis, E., A. V. Osipov, and T. F. Eibert, "Metamaterials for microwave radomes and the concept of a metaradome: Review of the literature," *International Journal of Antennas and Propagation*, Vol. 2017, 13 pages, 2017.
15. Sahu, B., P. Tripathi, and S. P. Singh, "Investigation on cylindrical dielectric resonator antenna with metamaterial superstrate," *Wireless Personal Communications*, Vol. 84, No. 2, 1151–1163, 2015.
16. Capolino, F., *Theory and Phenomena of Metamaterials*, CRC Press, 2009.
17. Veselago, V., L. Braginsky, V. Shklover, and C. Hafner, "Negative refractive index materials," *Journal of Computational and Theoretical Nanoscience*, Vol. 3, No. 2, 1–30, 2006.
18. Arora, C., S. S. Pattnaik, and R. N. Baral, "SRR superstrate for gain and bandwidth enhancement of microstrip patch antenna array," *Progress In Electromagnetics Research B*, Vol. 76, 73–85, 2017.
19. Abdel-Rahman, A. B. and A. A. Ibrahim, "Metamaterial enhances microstrip antenna gain," *Microwave & RF*, 46–50, August 2015.
20. Chaimool, S., K. L. Chung, and P. Akkaraekthalin, "Simultaneous gain and bandwidths enhancement of a single-feed circularly polarized microstrip patch antenna using a metamaterial reflective surface," *Progress In Electromagnetics Research B*, Vol. 22, 23–37, 2010.
21. Abdelrehim, A. A. A. and H. Ghafouri-Shiraz, "Performance improvement of patch antenna using circular split ring resonators and thin wires employing metamaterials lens," *Progress In Electromagnetics Research B*, Vol. 69, 137–155, 2016.
22. Moretti, E. A., R. Anholon, I. S. Rampasso, D. Silva, L. A. Santa-Eulalia, and P. S. A. Ignacio, "Main difficulties during RFID implementation: An exploratory factor analysis approach," *Technology Analysis & Strategic Management*, Vol. 31, No. 8, 943–956, 2019.
23. Moreira, E. C., A. S. B. Sombra, and G. C. Barroso, "An UHF RFID reader antenna made of recycled and reutilized materials from construction debris," *IEEE 23rd International Symposium on Personal, Indoor and Mobile Radio Communications*, Sydney, NSW, 2012.
24. Chung, K. L. and A. Sanagavaparu, "A systematic design method to obtain broadband characteristics for singly-fed electromagnetically coupled patch antennas for circular polarization," *IEEE Transactions on Antennas and Propagation*, Vol. 51, No. 12, 3239–3248, 2003.
25. Costa, F., A. Monorchio, and G. Manara, "An overview of equivalent circuit modeling techniques of frequency selective surfaces and metasurfaces," *ACES Journal*, Vol. 29, No. 12, 960–976, 2014.
26. Gao, X., X. Yu, W. Cao, Y. Jiang, and X. Yu, "Ultra-wideband circular-polarization converter with micro-split Jerusalem-cross metasurfaces," *Chinese Physics B*, Vol. 25, No. 12, 128102, 2016.
27. Katiyar, P. R. and W. N. L. B. W. Mahadi, "Comparative analysis of different single cell metamaterial," *Australian Journal of Basic and Applied Sciences*, Vol. 8, No. 21, 1–7, 2014.
28. Vallecchi, A., F. Capolino, and A. G. Schuchinsky, "2-D isotropic effective negative refractive index metamaterial in planar technology," *IEEE Microwave and Wireless Components Letters*, Vol. 19, No. 5, 269–271, May 2009.
29. Majumdar, P., Z. Zhao, C. Ji, and R. Liu, "Parametric analysis and modeling of jerusalem cross frequency selective surface," *International Journal of Electromagnetics and Applications*, Vol. 6, No. 1, 13–21, 2016.
30. Quan, X., S. Zhang, and H. Li, "Metamaterials forge high-directivity antenna," *Microwave & RF*, Vol. 54, No. 6, 50–56, June 2015.
31. Wang, H., X. Chen, and K. Huang, "An improved approach to determine the branch index for retrieving the constitutive effective parameters of metamaterials," *Journal of Electromagnetic Waves and Applications*, Vol. 25, No. 1, 85–96, 2011.
32. Numan, A. B. and M. S. Sharawi, "Extraction of material parameters for metamaterials using a full-wave simulator," *IEEE Antennas and Propagation Magazine*, Vol. 55, No. 5, 202–211, 2013.

33. Payandehjoo, K. and R. Patton, "De-embeding the effect of a printed array of probes on planar very-near-field measurements," *2014 IEEE Conference on Antenna Measurements & Applications (CAMA)*, 1–4, Antibes Juan-les-Pins, 2014.
34. Patton, R., "A very-near-field measurement technique to test large antennas in the lab," *Microwave Journal*, Vol. 57, No. 1, 116–120, January 2014.
35. Silva, S. B. and A. R. Correia, "Minimum activation power of a passive UHF RFID tags: A low cost method," *Journal of Aerospace Technology and Management*, Vol. 10, Article ID e2418, 2018.